*Int. J. Electrochem. Sci.*, 15 **(2020)** 5018 – 5030, doi: 10.20964/2020.06.20

International Journal of
ELECTROCHEMICAL
SCIENCE
www.electrochemsci.org

# Glassy Carbon Electrodes Modified with Molybdenum Carbide ($Mo_xC_y$) and Decorated with Multiwalled Carbon Nanotubes for the Simultaneous Determination of Hydroquinone and O-Hydroxyaniline Levels

*Wenfeng Zhuge, Xueying Li, Xiaokun Li*[*]*, and Suxiang Feng*

School of Pharmacy, Henan University of Traditional Chinese Medicine, Zhengzhou 450046, China
[*]E-mail: li96052122@126.com

*Received:* 6 December 2019 / *Accepted:* 5 February 2020 / *Published:* 10 May 2020

A sensitive electrochemical sensor decorated with multiwalled carbon nanotubes and molybdenum carbide (MWCNTs-$Mo_xC_y$) was successfully developed in this study for the simultaneous detection of hydroquinone (HQ) and o-hydroxyaniline (OHX). The MWCNTs-$Mo_xC_y$ nanomaterials were synthesized by high temperature calcination under nitrogen protection, and the morphologies and elements were characterized and analyzed using a scanning electron microscope (SEM) and energy dispersive spectrometry (EDS), respectively. The MWCNTs-$Mo_xC_y$ composite was ultrasonically dispersed into a modification liquid to construct the modified the glassy carbon electrode, and cyclic voltammetry (CV), differential pulse voltammetry (DPV) and chronocoulometry (CC) were used to study the electrochemical performance. In phosphate buffer solution, the synthetic materials displays good redox peaks for hydroquinone (HQ) and o-hydroxyaniline (OHX). The synthesized composite has a large effective surface area, high electron transfer rate and catalytic activity. Under optimum experimental conditions, the MWCNTs-$Mo_xC_y$/GCE exhibits linear responses to HQ and OHX in the range of 0.1-900.0 μM and 0.8-20.0 μM, respectively, with a limit of determination (S/N=3) calculated to be 0.075 μM and 0.047 μM, respectively. The method was applied to measure the concentrations of these compounds in real water samples and achieved satisfactory results.

**Keywords:** Multi-walled carbon nanotube; carbon molybdenum compound; hydroquinone; o-hydroxyaniline, cyclic voltammetry; differential pulse voltammetry

## 1. INTRODUCTION

Hydroquinone (HQ) and o-hydroxyaniline (OHX) (also known as o-aminophenol, OAP) are present in phenolic compounds and are common industrial raw materials used to prepare fine chemicals, agricultural drugs, synthetic dyes, coal mining, etc. [1,2]. However, they are environmental

pollutants that not only affect the growth and development of animals and plants, but also harm human life and health [3,4]. HQ is a high-temperature decomposable toxic compound. If it is accidentally consumed by adults in quantities greater than 1.0 g, the person will experience headache, dizziness, stomachache, tinnitus, a pale complexion and an aggravation of rheumatoid arthritis [5,6]. OHX is an allergenic substance that can cause tracheal diseases and contact dermatitis. Once a large amount of OHX is inhaled, it increases the accumulation of human hepatic toxins and even damages the kidneys in the human body [7,8]. The discharge of these phenolic substances into the environment will cause substantial damage to the organism. For example, the use of water containing HQ or OHX to irrigate crops can lead to reduced yields and even wilting of crops, and cause the death of aquatic organisms. The toxicity of waste water containing HQ or OHX also inhibits the growth rate of other organisms in the water, and these compounds are difficult to biodegrade, subsequently disrupting the natural ecological balance and causing irreversible damage [9-12]. Because phenolic compounds not only pollute water bodies but also pose a threat to human health, the US Environmental Protection Agency and the European Union have included phenolic compounds in the ranks of environmental pollutants [13,14]. Research has gradually focused on environmental protection departments and corporate waste water testing to establish an approach to detect phenolic pollutants in water bodies. Therefore, a method for the simultaneous detection of HQ and OHX must be developed.

In recent years, many analytical technologies have been applied to analyze HQ or OHX, such as electrochemical analysis [15-18], spectrophotometry [19-21], high-performance liquid chromatography [22-24], and gas chromatography [25-27]. However, spectrophotometry, high-performance liquid chromatography and gas chromatography usually require sophisticated instruments and expert operators, resulting in high cost and time-consuming analyses. Due to its good stability, high sensitivity, low limit of detection and low cost, electrochemical sensing technology has received increasing attention in the field of chemical analysis, biomedicine, food safety and environmental monitor recently [28-34]. Molybdenum carbide ($Mo_xC_y$) have the same catalytic capacity as noble metals, such as Ag, Pt and Pd. Unlike platinum precious metals, $Mo_xC_y$ has the advantages of sulfur and carbon dioxide resistance and sintering resistance; meanwhile, it displays excellent catalytic activity and selectivity [35-37] and is a low-cost catalyst compared to expensive metal materials [38]. However, $Mo_xC_y$ has a small specific surface area and a weak electrical conductivity, limiting its applications in the field of catalysis. The carbide is generally complexed with a material having a relatively large specific surface area to completely utilize the catalytic activity of molybdenum carbide [39]. The covalent bonds of multiwalled carbon nanotubes (MWCNTs) are the most stable covalent bond in nature, and MWCNTs possess a unique structure and good mechanical properties [40]. Moreover, MWCNTs have extremely high strength, strong toughness and excellent conductivity [41,42]. In addition, MWCNTs have an ultra-high nanoscale void layout and specific surface area, which provides a large number of absorption sites [43,44].

Here, using MWCNTs as carbon source and ammonium molybdate as source of molybdenum, the MWCNTs were initially activated by nitric acid, subjected to an ultrasonication treatment for even dispersion, and then reacted with ammonium molybdate at a high temperature under the protection of nitrogen to generate MWCNTs-$Mo_xC_y$ compounds [45]. Glassy carbon electrodes (GCEs) was modified with these compounds for electrochemical detection. The MWCNTs-$Mo_xC_y$/GCE displays a

strong catalytic capacity, enhanced electrical conductivity, a greater number of active sites and larger specific surface area, and thus can be used for the simultaneous detection of HQ and OHX.

## 2. EXPERIMENTAL SECTION

### *2.1. Reagents and apparatus*

$(NH_4)_6Mo_7O_{24}\cdot 4H_2O$ was acquired from Tianjin chemical Reagent NO. 4 Plant Kaida Chemical Plant (Tianjin, China). MWCNTs were obtained from Shenzhen Nanomaterials Port Co., Ltd. (Guangdong, China). The hydroquinone (HQ) standard was purchased from Shantou Xilong Chemical Plant Co., Ltd. (Guangdong, China). The O-hydroxyaniline (OHX) standard was acquired from Aladdin (Shanghai, China). A 0.1 M phosphate buffer (PB) solution was used as the supporting electrolyte, which was prepared from disodium phosphate dodecahydrate and sodium dihydrogen phosphate. The pH of the electrolyte was adjusted to 4.0-9.0 by adding 0.1 M HCl. The water samples were collected from Guangxi Normal University for Nationalities (Chongzuo, China). All other reagents were of analytical grade. Electrochemical experiments were conducted at room temperature. Deionized water was used in all experiments.

The MWCNTs-$Mo_xC_y$ morphologies and elements were characterized and analyzed using a scanning electron microscope (SEM, ZEISS EVO 18, Carl Zeiss AG, Germany). All electrochemical experiments were performed using a CHI660E electrochemical workstation (Shanghai Chenhua instrument Co., Ltd. China) with three-electrode system, in which a glassy carbon electrode (GCE, Φ=3 mm) was used as the working electrode, the reference electrode was a calomel electrode and the auxiliary electrode was a platinum wire electrode.

### *2.2. MWCNTs pretreatment*

Five grams of MWCNTs were placed in a round bottom flask with 200 mL of concentrated nitric acid, as measured with a cylinder, and heated to 130°C for 6 h with constant stirring. After cooling to room temperature, the solution was filtered with a Buchner funnel, washed with deionized water until a neutral pH was obtained, and finally placed in a blast drying oven and dried at 100°C for 12 h.

### *2.3. Preparation of MWCNTs-$Mo_xC_y$*

First, 1.36 g of pretreated MWCNTs and 0.96 g of $(NH_4)_6Mo_7O_{24}\cdot 4H_2O$ were mixed with a 20 mL deionized water and sequentially sonicated for 2 h. After using an electric heater to remove the moisture and placing the mixture in a blast drying oven and drying it at 100°C for 3 h, the dried sample was transferred to a tube furnace under a nitrogen stream as protective gas and then high temperature calcination was performed for 3 h (temperature program setting: the mixture was heated to 1000°C at a rate of 5°C·min$^{-1}$, maintained at a constant temperature for 3 h, and then cooled to 300°C at a rate of

5°C·min$^{-1}$). The complexes were naturally cooled to room temperature under a nitrogen atmosphere and maintained in this state for 10 h.

### *2.4. Preparation of modified electrodes*

The glassy carbon electrode was polished to a mirror-like surface with a solution containing 0.3 μm-0.5 μm aluminum oxide powder and cleaned with deionized water, after drying under infrared light. Using deizonized water as the solvent, MWCNTs-$Mo_xC_y$ and MWCNTs were dispersed into 1.0 mg·mL$^{-1}$ suspensions, respectively. Five microliters of the MWCNTs-$Mo_xC_y$ suspensions were coated on the surface of the GCE. Three microliters of 5 Wt% chitosan was coated on the electrode modified with MWCNTs-$Mo_xC_y$/GCE and thoroughly dried under infrared light to increase the stability of the electrochemical sensor. The same method and concentration were used to simultaneously prepare MWCNTs/GCE and Bare/GCE contrast electrodes.

## 3. RESULTS AND DISCUSSION

### *3.1. Characterization of the prepared MWCNTs-$Mo_xC_y$ and MWCNTs*

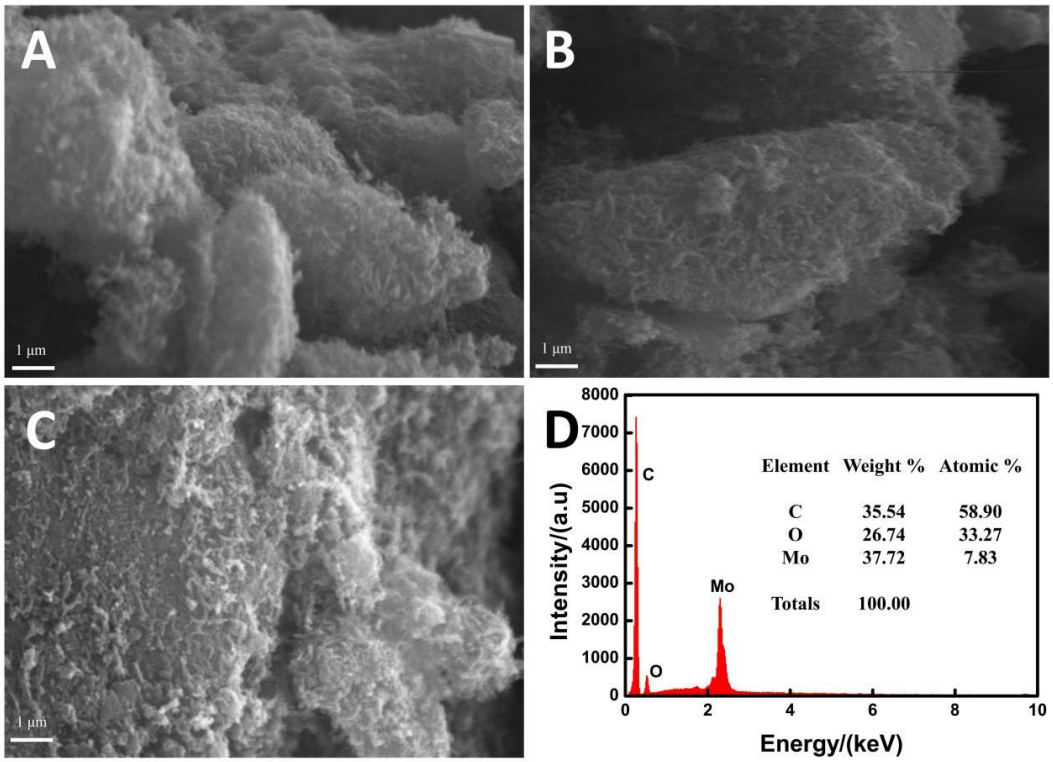


**Figure 1.** SEM images of the surface of (A-B) MWCNTs-$Mo_xC_y$ and (C) MWCNTs. The (D) EDS of MWCNTs-$Mo_xC_y$ is shown.

The surface morphologies of MWCNTs-$Mo_xC_y$ and MWCNTs were studied using the SEM

technique, and the results of the characterization are shown in Fig. 1. As shown in Fig. 1C, the surface of the MWCNTs was rough and unevenly distributed. In Fig. 1B-C, the composites were uniformly distributed, indicating that they may have a large specific surface area [46]. Based on the EDS shown in Fig. 1D, MWCNTs-$Mo_xC_y$ were successfully synthesized at a high temperature under nitrogen protection. The complex contains three elements, Mo, O and C. The molybdenum compounds containing O may be molybdenum oxides $MoO_3$, $MoO_2$ and MoO, and the molybdenum carbide compound is readily oxidized upon exposure to air.

### *3.2. Electrooxidation behaviors of HQ and OHX*

The electrochemical behaviors of different electrodes in pH 7.0 PB solution were investigated using cyclic voltammetry (CV). Fig. 2A shows the CVs of Bare/GCE, MWCNTs/GCE, MWCNTs-$Mo_xC_y$/GCE in a 0.1 M PB blank solution.

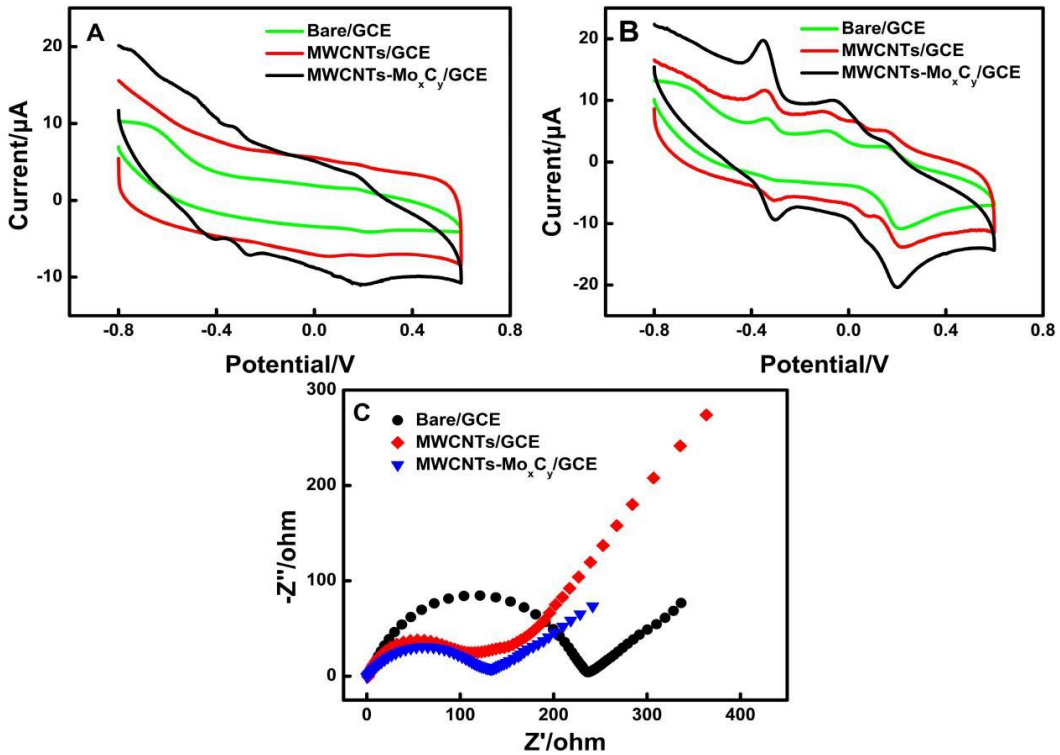


**Figure 2.** (A-B) CVs of Bare/GCE, MWCNTs/GCE and MWCNTs-$Mo_xC_y$/GCE in 0.1 M PB solution containing 20.0 mM HQ and 8.0 mM OHX; scan rate: 0.1V $s^{-1}$. (C) EIS of different modified electrodes in 5.0 mM potassium ferricyanide and potassium ferrocyanide solutions containing 0.1 M potassium chloride.

The voltammograms of Bare/GCE and MWCNTs/GCE did not present peaks, whereas the voltammogram of MWCNTs-$Mo_xC_y$/GCE contained some peaks attributed to molybdenum carbide. In the presence of 20.0 mM HQ and 8.0 mM OHX, the three modified electrodes displayed two obvious redox peaks, and a specific oxidation peak. As shown in Fig. 2B, the reactions with HQ and OHX were reversible processes. In this analysis, two oxidation peaks appeared at 0.21 V (HQ, 4.78 μA) and -0.31

V (OHX, 0.37 μA) in the CV of the Bare/GCE, respectively. For MWCNTs/GCE, the peak currents of HQ and OHX were 4.28 μA and 1.66 μA, and the peak currents of HQ and OHX were 9.59 μA and 4.58 μA for the MWCNTs-$Mo_xC_y$/GCE. A potential explanation for these results is that MWCNTs had excellent electrical conductivity, the MWCNTs-$Mo_xC_y$ composite combining the advantages of MWCNTs and $Mo_xC_y$ displayed an increase in the electrical conductivity, and thus the MWCNTs-$Mo_xC_y$/GCE exhibited excellent electrocatalysis toward HQ and OHX.

Electrochemical impedance spectroscopy (EIS) was used to investigate the electron transfer between the electrolyte and modified electrodes at an initial potential of 0.20 V as the open circuit potential. The EIS of modified electrodes in a 5.0 mM potassium ferricyanide and potassium ferrocyanide solution containing 0.1 M potassium chloride is shown in Fig. 2C. The composition of the ideal impedance map should be a higher frequency semicircle and a straight line in a lower frequency range. The semicircle in the high frequency region reflects the activation of the material, the straight line in the low frequency region reflects the mass transfer rate, and the diameter ($R_t$) of the semicircle represents the transfer rate of electrons [47]. The order of $R_t$ for each electrode was: $R_{MWCNTs}$< $R_{MWCNTs\text{-}MoxCy}$< $R_{Bare}$. A potential explanation for the result is that the MWCNTs exhibited strong electrical conductivity, the impedance they received during the reaction was poorer, and the $Mo_xC_y$ possessed weak electrical conductivity. Therefore, the electrical conductivity of MWCNTs-$Mo_xC_y$/GCE was less than MWCNTs/GCE. Moreover, the diameter of MWCNTs-$Mo_xC_y$/GCE was smaller than Bare/GCE, indicating that MWCNTs-$Mo_xC_y$ promoted faster electron transfer on the electrode surface.

### *3.3. Optimization of pH*

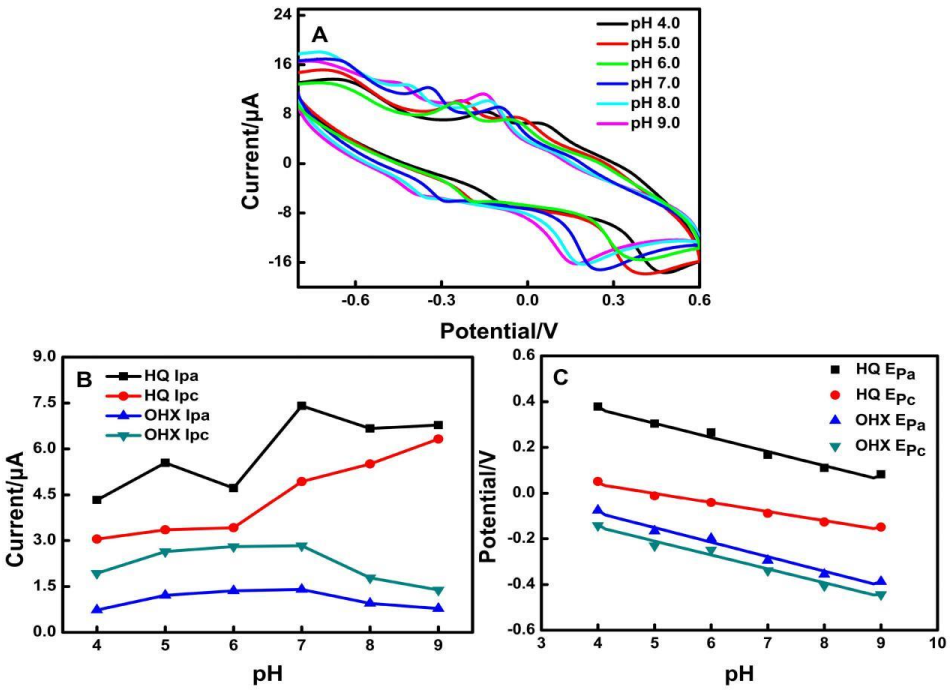


**Figure 3.** CVs of MWCNTs-$Mo_xC_y$/GCE in solutions with different pHs (4.0, 5.0, 6.0, 7.0, 8.0, 9.0) containing HQ 20.0 mM and OHX 8.0 mM (A). Plots of the peak current and peak potential vs. the pH values are shown (B and C). Scan rate: 0.1 $V \cdot s^{-1}$

The effect of pH values ranging from 4.0-9.0 on the peak current and peak potential of 20.0 mM HQ and 8.0 mM OHX was analyzed using CV. As shown in Fig. 3A and 3B, the oxidation peak current of HQ and OHX gradually increased as the pH increased, and gradually decreased when the pH reached the maximum value of 7.0. The peak potential (Ep) also changed as the pH increased. The linear relationship between the oxidation peak of HQ and pH was expressed as Epa = -0.062 pH+0.69 (r = 0.9902), and the linear relationship between the oxidation peak of OHX and pH was expressed as Epa = -0.064 pH+0.17 (r = 0.9901). At a pH of 7.0, HQ and OHX displayed a better response, with the strongest oxidation peak and the largest separation between peaks. Therefore, a PB solution with a pH of 7.0 was selected as the supporting electrolyte. The absolute value of slope of the linear relationship between HQ oxidation peak and pH value was 61.6 $mV \cdot pH^{-1}$, which was similar to the theoretical value (59.2 $mV \cdot pH^{-1}$), indicating that the number of electrons transferred ($n_1$) in the HQ electrochemical reaction was equal to the number of protons transferred ($m_1$). Similarly, the number of electrons transferred ($n_2$) in the OHX electrochemical reaction was equal to the number of protons transferred ($m_2$).

### *3.4. Effect of scan rates*

Under optimized conditions, CV was used to study the effect of the scanning rate on MWCNTs-$Mo_xC_y$/GCE in a PB solution containing 20.0 mM HQ and 8.0 mM OHX, and the scanning rate ranged from 0.1 to 1.0 $V \cdot s^{-1}$. The results are presented in Fig. 4A. The oxidation and reduction peaks of HQ and OHX increased as the scanning speed increased. A good linear relationship was observed between the peak current and the scan rate of the two materials, as shown in Fig. 4B. The linear equation of HQ was expressed as Ipa (μA) = -7.99 ν ($V \cdot s^{-1}$)-5.92 (r= 0.9909), Ipc (μA) = 2.82 ν ($V \cdot s^{-1}$)+2.48 (r= 0.9956). The liner equation of OHX was expressed as Ipa (μA) = -7.14 ν ($V \cdot s^{-1}$)-1.96 (r= 0.9955), Ipc (μA) = 10.62 ν ($V \cdot s^{-1}$)+3.26 (r= 0.9968). The linear relationship between the peak current (Ip) and scan rate (ν) indicates that HQ and OHX are adsorption-controlled processes on the target-modified electrode [48].

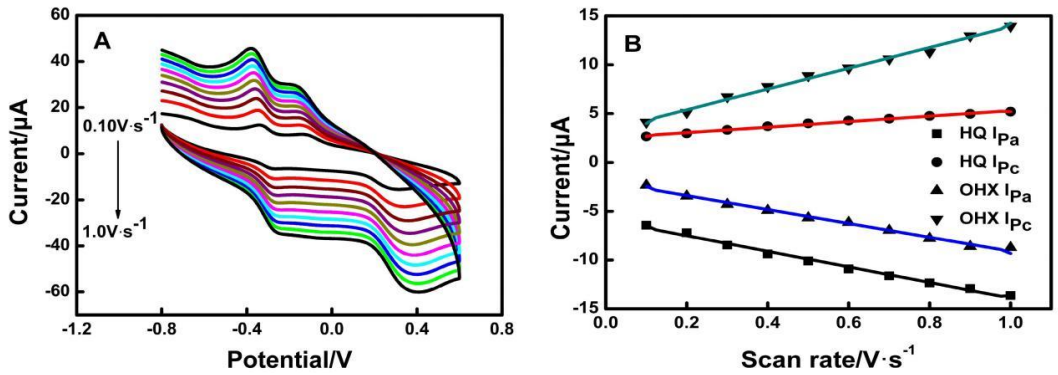


**Figure 4.** (A) CVs of a mixture of 20.0 mM HQ and 8.0 mM OHX in 0.1 M PB (10.0 mL) on MWCNTs-$Mo_xC_y$/GCE at different scan rates (0.1-1.0: 0.1, 0.2, 0.3, 0.4, 0.5, 0.6, 0.7, 0.8, 0.9, and 1.0 $V \cdot s^{-1}$) in PB solution. (B) Peak current (Ip) vs. the square root of the scan rate (ν).

*3.5. Individual and simultaneous measurement of HQ and OHX levels*

HQ and OHX were simultaneously detected using differential pulse voltammetry (DPV) under optimal conditions. As shown in Fig. 5A-G, the oxidation peak potentials were HQ (0.052 V) and OHX (-0.328 V).

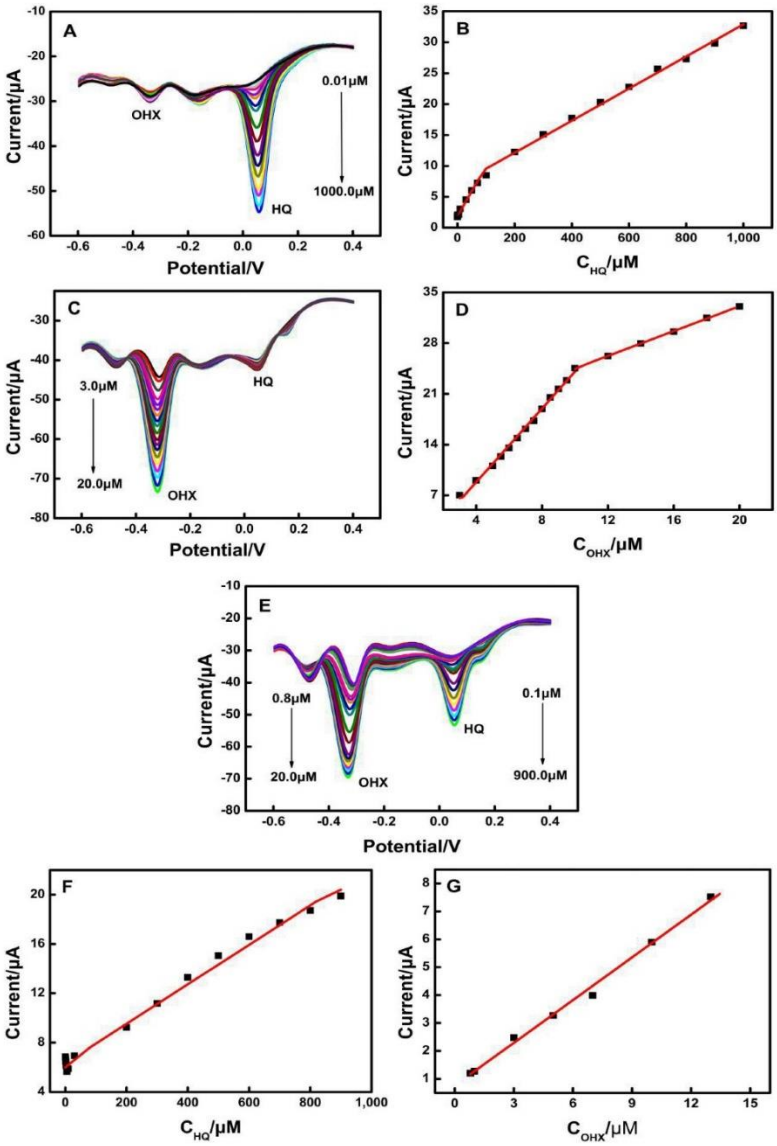


**Figure 5.** DPV curves for MWCNTs-$Mo_xC_y$/GCE in 0.1 M PB (10.0 mL) containing (A) 1.0 μM OHX and different concentrations of HQ ranging from 0.01 to 1000.0 μM or (C) 40.0 μM HQ and different concentrations of OHX ranging from 3.0 μM to 20.0 μM. Plots of the oxidation peak current versus the concentrations of HQ (B) and OHX (D) are shown. (E) DPV curves recorded during the simultaneous detection of HQ and OHX by MWCNTs-$Mo_xC_y$/GCE in 0.1 M PB (10.0 mL) with HQ concentrations ranging from 0.1 to 900.0 μM and OHX concentrations ranging from 0.8 to 20.0 μM in the mixed solution. (F) and (G) Plots of the oxidation peak currents versus various concentrations of HQ and OHX, respectively.

First, the concentration of OHX was fixed at 1.0 μM, and different concentrations of HQ were successively added to the PB solution. As shown in Fig. 5A and 5B, as the HQ concentration increased,

its oxidation peak current also gradually increased. In the concentration range of 0.01 to 1000.0 μM, the peak current of HQ showed a good piecewise linear relationship with its concentration, and the linear equations were expressed as I (μA) = 0.080 C (μM)+1.89 (r= 0.9954) and I (μA) = 0.026 C (μM)+6.95 (r= 0.9977), with detection limits of 0.008 μM.

Next, the concentration of HQ was fixed at 40.0 μM, and different concentrations of OHX were successively added to the PB solution. As shown in Fig. 5C and 5D, as the OHX concentration increased, its oxidation peak current also gradually increased. In the concentration range of 3.0 μM to 20.0 μM, the peak current of OHX showed a good piecewise linear relationship with its concentration, and the linear equations were expressed as I (μA) = 2.54 C (μM)-1.37 (r= 0.9956) and I (μA) = 0.86 C (μM)+15.94 (r= 0.9998), with a detection limit of 0.111 μM.

Finally, we simultaneously measured the relationship between the oxidation peak current of HQ and OHX in the mixture as the concentration changed, as shown in Fig. 5E-G. When the concentration of HQ ranged from 0.1 μM to 900.0 μM, its peak current displayed a good linear relationship with its concentration, and the linear equation was expressed as I (μA) = 0.016 C (μM)+6.32 (r= 0.9954), with a detection limit of 0.075 μM. When the concentration of OHX ranged from 0.8 μM to 20.0 μM, the peak current displayed a good liner relationship with its concentration, and the linear equation was expressed as I (μA) = 0.51 C (μM)+7.60 (r= 0.9974), with a detection limit of 0.047 μM. The MWCNTs-$Mo_xC_y$/GCE exhibited good sensitivity and a low limit of detection during the simultaneous measurement of HQ and OHX levels, without interference.

The developed method was compared with similar sensors that have been reported early for determination of HQ or OHX. The outstanding characteristics of the developed method are summarized in Table 1. As can be seen, the proposed sensor exhibits excellent limits of detection and linear range for HQ and OHX.

**Table 1.** Comparison of analytical performances at various electrodes reported earlier for determination of HQ and OHX

| Electrode | Linear range (μM) | | Detection limit (μM) | | In the presence of other analytes | Refs. |
|---|---|---|---|---|---|---|
| | HQ | OHX | HQ | OHX | | |
| PI/RGO-AuNPs[a)] | 1 - 654 | - | 0.09 | - | catechol | 49 |
| AuNPs/RGO[b)]/$WO_3$ | 0.1 - 10 | - | 0.036 | - | catechol | 50 |
| Pd/Poly(TAU)[c)]/GCE | 0.01 - 100 | - | 0.01 | - | catechol | 51 |
| $Ti_3C_2$-MWCNTs/GCE | 2 - 150 | - | 0.0066 | - | catechol | 52 |
| SPEs[d)] | 0.5 - 10 | - | 0.185 | - | paracetamol, estradiol | 53 |
| MWCNTs-$Mo_xC_y$/GCE | 0.1 - 900.0 | 0.8 - 20.0 | 0.075 | 0.047 | - | this work |

a) polyimide/reduced graphene oxide-Au nanoparticles. b) reduced grapheme oxide. c) Pd nanoparticles/poly (taurine) film. d) carbon screen-printed electrodes

### *3.6. Reproducibility and stability of the electrode*

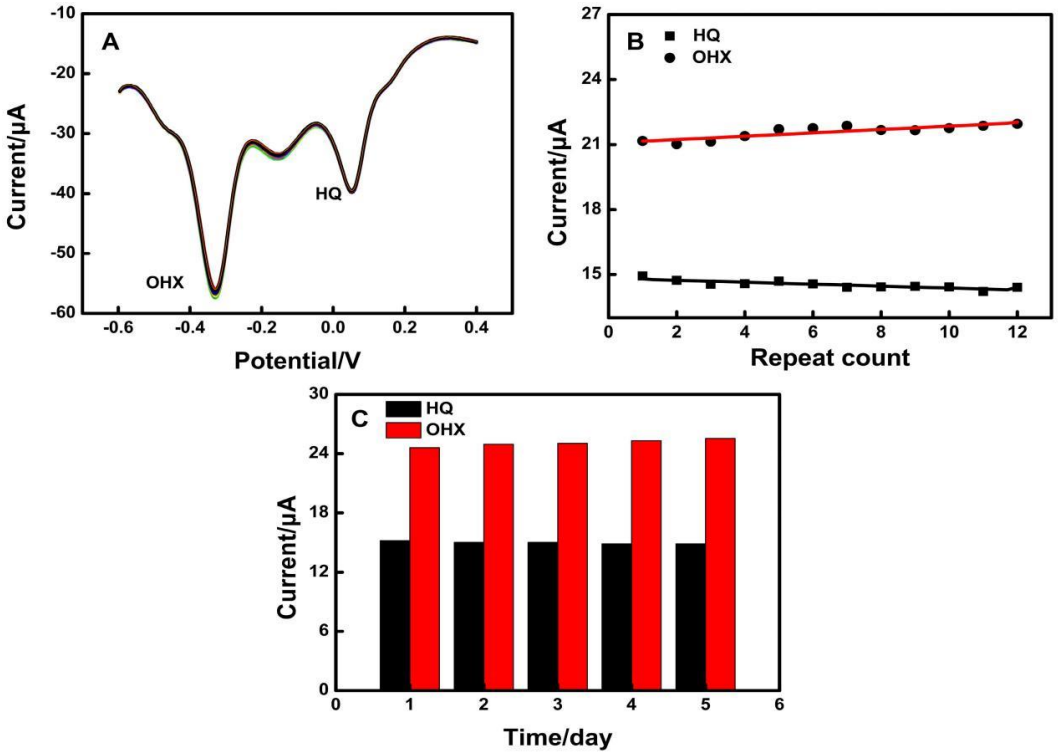


**Figure 6.** The reproducibility (A-B) and stability (C) of MWCNTs-$Mo_xC_y$/GCE were analyzed by performing repeated measurements of the DPV response to 200.0 μM HQ and 10.0 μM OHX in 10.0 mL PB.

Under optimal conditions, the reproducibility and stability of MWCNTs-$Mo_xC_y$/GCE were studied. DPV was used 12 times in the presence of 200.0 μM HQ and 10.0 μM OHX, and the relative standard deviations (RSDs) were 1.30% and 1.22%, respectively. As shown in Fig. 5A and Fig. 5B, the modified MWCNTs-$Mo_xC_y$/GCE displayed good reproducibility. In addition, the stability of MWCNTs-$Mo_xC_y$/GCE was determined using DPV under the optimal experimental conditions. The peak current of the electrode in PB containing 200.0 μM HQ and 10.0 μM OHX was determined on five consecutive days. After each test, the MWCNTs-$Mo_xC_y$/GCE was first washed with distilled water and soaked in absolute ethanol for 10 min, dried under an infrared lamp, and then stored in a refrigerator. By comparing the current peaks measured over successive days, the relative standard deviations of HQ and OHX were 0.93% and 1.41%, respectively. As shown in Fig. 5C, the prepared MWCNTs-$Mo_xC_y$/GCE displayed good stability.

### *3.7. Electrode interference experiment*

Some potential interfering substances, such as nitrates and chlorine compounds, were detected at an applied potential of -0.6-0.4 V to further confirm the lack of interference of other compounds in actual samples on the performance of the prepared MWCNTs-$Mo_xC_y$/GCE sensor. The effects of potassium chlorate, urea, barium sulfate, muriate, potassium nitrate, sodium nitrite, sodium nitrate, ethanedioic acid, sodium bicarbonate, sodium chloride, manganese sulfate, ammonium sulfate,

magnesium chloride hexahydrate, calcium carbonate, potassium hydroxide, p-phthalic acid, phenol and p-nitrophenol at 100 times the concentrations of HQ on HQ and OHX were studied using DPV. With the exception of the interference of catechol in the detection of HQ, the interference of the above-mentioned remaining substances in the detection of the current resulting from the reaction with the target substance was negligible.

### *3.8. Analysis of real samples*

Under the optimal conditions, real samples from three different lake were analyzed by this method. In the linear range established for the simultaneous determination of HQ and OHX, the contents of these compounds in three water samples were measured using the standard addition method, and the recovery of spiked compounds was calculated. The experimental results of the test are shown in Table 2. The range of recoveries for spiked samples used to determine water quality in these three areas was 95.00% to 105.00%, and the relative standard deviation (<5.00%) met the experimental requirements.

**Table 2.** Determination of the recovery of HQ and OHX

| Sample | HQ | | | | OHX | | | |
|---|---|---|---|---|---|---|---|---|
| | Detect M | Added $10^{-4}$ M | Recovery % | RSD % | Detect M | Added $10^{-5}$ M | Recovery % | RSD % |
| 1# | - | 5.50 | 101.49 | 0.71 | - | 2.70 | 103.74 | 0.71 |
| 2# | - | 5.50 | 102.47 | 0.28 | - | 2.70 | 100.96 | 2.07 |
| 3# | - | 5.50 | 104.01 | 0.89 | - | 2.70 | 96.80 | 1.02 |

1# real samples from the west lake, 2# real samples from the east lake, 3# real samples from the jinlong lake.

## 4. CONCLUSIONS

In this experiment, an electrochemical sensor based on the MWCNTs-$Mo_xC_y$ composite modified glassy carbon electrode was applied for the simultaneous detection of HQ and OHX. The MWCNTs-$Mo_xC_y$ material possesses a strong conductivity and good catalytic performance, and contains numerous active sites. Under the optimum experimental conditions, the MWCNTs-$Mo_xC_y$/GCE are highly sensitive and show good selectivity, stability and reproducibility in the simultaneous detection of HQ and OHX. A good linear relationship was observed for concentrations of HQ and OHX ranging from 0.1-900.0 μM and 0.8-20.0 μM, with limits of detection as low as 0.075 μM and 0.047 μM, respectively. The results of the analysis of real samples confirmed the potential application of the MWCNTs-$Mo_xC_y$ composite in the simultaneous the detection of HQ and OHX levels in water samples.

## References

1. X. Huang, X. Deng, W. Qi, D. Wu, *J. Nanosci. Nanotechno*., 18 (2018) 8118.

2. Y.-H. Huang, J.-H. Chen, L.-J. Ling, Z.-B. Su, X. Sun, S.-R. Hu, W. Weng, Y. Huang, W.-B. Wu, Y.-S. He, *Analyst*, 140 (2015) 7939.
3. Y. Liu, Y.-M. Wang, W.-Y. Zhu, C.-H. Zhang, H. Tang, J.-H. Jiang, *Anal. Chim. Acta*, 1012 (2018) 60.
4. J. Teng, X. Hu, N. Tao, M. Wang, *Front. Agr. Sci. Eng*., 5 (2018) 321.
5. Y. Dang, Y. Zhai, L. Yang, Z. Peng, N. Cheng, Y. Zhou, *Chem. Commun*., 6 (2016) 83994-84002.
6. M. Nazari, S. Kashanian, P. Moradipour, N. Maleki, *J. Electroanal. Chem*., 812 (2018) 122.
7. H. Tian, Y. Hu, X. Xu, M. Hui, Y. Hu, W. Qi, H. Xu, B. Li, *Bioresource technol*., 289 (2019) 121649
8. T. Gong, P. Li, Q. Sui, J. Chen, J. Xu, E.-Q. Gao, *J. Mater. Chem.* A, 6 (2018) 9236.
9. C. N. Jen, Y. Liang, L. E. Hatch, N. M. Kreisberg, C. Stamatis, K. Kristensen, A. H. Goldstein, *Environ. Sci. Tech. Let*., 5 (2018) 309.
10. M. Velmurugan, N. Karikalan, S.-M. Chen, Y.-H. Cheng, C. Karuppiah, *J. Colloid Interf. Sci*., 500 (2017) 54-62.
11. G. Mo, X. He, C. Zhou, D. Ya, J. Feng, C. Yu, B. Deng, *Sensor. Actuat. B-Chem*., 266 (2018) 784.
12. Y. Yi, G. Zhu, X. Wu, K. Wang, *Biosens. Bioelectron*., 77(2016) 353-358.
13. C.-C. Gu, X.-P. Li, H.-Y. Liu, *J. Nano Res*., 54 (2018) 42.
14. H. Hammani, F. Laghrib, S. Lahrich, A. Farahi, M. Bakasse, A. Aboulkas, M. A. El Mhammedi, *Ionics*, 25 (2018) 2285.
15. S. R. Kim, S. Cho, M. I. Kim, *J. Nanosci. Nanotechno*., 18 (2018) 1246.
16. G. B. Braga, A. E. F. Oliveira, A. C. Pereira, *Electroanal*., 30 (2018) 2176.
17. Y. Li, H.-Y. Bi, X.-M. Mao, Y.-Q. Liang, H. Li. *Appl. Clay Sci*., 162 (2018) 230.
18. R. A. Senthil, A. Selvi, P. Arunachalam, L. S. Amudha, J. Madhavan, A. M. Al-Mayouf, *J. Mater. Sci.- Mater.-El.*, 28 (2017) 10081.
19. L. Tong, Q. Chen, A. A. Wong, R. Gómez-Bombarelli, A. Aspuru-Guzik, R. G. Gordon, M. J. Aziz, *Phys. Chem. Chem. Phys*., 19 (2017), 31684.
20. M. Esteki, S. Nouroozi, Z. Shahsavari, *Int. J. Cosmetic Sci*., 38 (2016) 25-34.
21. A. I. Marakhova, *Russ. Chem. Bull*., 64 (2015) 1267.
22. B. Farajmand, M. Esteki, E. Koohpour, V. Salmani, *J. Sep. Sci.,* 40 (2017）1524.
23. C.-S. Lu, S.-D. Huang, *J. Chromatogr*. A, 696 (2011) 201.
24. H. Ma, F. Mu, S. Fan, X. Zhou, Q. Jia, *J. Sep. Sci*., 35 (2012) 2484.
25. M. A. Farajzadeh, A. Yadeghari, L. Khoshmaram, H. Ghorbanpour, *J. Sep. Sci.,* 37 (2014) 2966.
26. J. I. Cacho, N. Campillo, P. Vinas, M. Hernández-Córdoba, *Food Chem*., 200 (2016) 249.
27. A. I. Abiola, H. Arsad, M. R. Samian, *Pharmacogn. Mag*., 14 (2018) 191.
28. J. Peng, Q. Huang, W. Zhuge, Y. Liu, C. Zhang, W. Yang, G. Xiang, *Biosensor. Bioelectron*., 106 (2018) 212.
29. J. Peng, W. Zhuge, Y. Huang, C. Zhang, W. Huang, *B. Korean Chem. Soc.,* 40 (2019) 214.
30. J. Peng, Q. Huang, Y. Liu, F. Liu, C. Zhang, Y. Huang, W. Huang, *J. Chin. Chem. Soc*., 66 (2019) 1311.
31. J. Peng, Q. Huang, Y. Liu, P. Liu, C. Zhang, *Sensor. Actuat. B-Chem.,* 294 (2019) 157.
32. F.. Liu, Q. Xu, W. Huang, Z. Zhang, G. Xiang, C. Zhang, C. Liang, H. Lian, J. Peng, *Electrochim. Acta*, 295 (2019) 615.
33. J. Peng, W. Zhuge, Y. Liu, C. Zhang, W. Yang, Y. Huang, *J. Electrochem. Soc*., 166 (2019) B1612.
34. J. Peng, C. Hou, X. Hu, *Sensor. Actuat. B-Chem*., 169 (2012) 81.
35. G. Yan, X. Feng, S. U. Khan, L. Xiao, W. Xi, H. Tan, Y. Ma, L. Zhang, Y. Li, *Chem.-Asian J.,* 13 (2018) 158.
36. Y. Wang, S. Zhu, N. Tsubaki, M. Wu., *ChemCatChem*, 10 (2018) 2300.
37. L. He, Y. Qin, H. Lou, P. Chen, *RSC Adv.,* 5 (2015) 43141.
38. D. H. Youn, S. Han, J. Y. Kim, H. Park, S. H. Choi, J. S. Lee, *ACS Nano*, 8 (2014) 5164.
39. J. Du, C. Song, J. Zhao, Z. Zhu, *Appl. Surf. Sci*., 255 (2008) 1989.

40. S. Zeng, P. Duan, M. Shen, Y. Xue, F. Lu, L. Yang, *Compos. Interface*., 26 (2018) 291.
41. A. Bouhamed, C. Müller, S. Choura, Q. Kanoun, *Sensor. Actuat. A-Phys*., 257(2017) 65.
42. C. Lv, Z. Huang, Q. Yang, C. Zhang, *J. Alloy. Compound*., 750 (2018) 927.
43. B. Wang, Y. Xing, J. Li, *J. Wuhan Univ. Technol*., 33 (2018) 102.
44. M. K. M. Nodeh, M. R. Haghighi, S. Soltani, H. R. Nodeh, *J. Liq. Chromatogr. Relat. Technol*., 41 (2018) 239.
45. F. Wang, J. Jiang, K. Wang, Q. Zhai, H. Sun, P. Liu, J. Feng, H. Xia, J. Ye, Z. Li, F. Li, J. Xu, *Fuel*, 228 (2018) 103.
46. J.-Y. Yang, X.-Y. Jiang, F.-P. Jiao, J.-G. Yu, *Appl. Surf. Sci*., 436 (2018) 198.
47. Q. Huang, X. Li, S. Feng, W. Zhuge, F. Liu, J. Peng, S. Mo, *Anal. Methods-UK*, 10 (2018) 3594.
48. Y. Peng, Z. R. Tang, Y. P. Dong, G Che, Z. F. Xin, *J. Electroanal. Chem*., 846 (2018) 38.
49. X. Shen, X. Xia, Y. Du, C. Wang, *Front. Mater. Sci.*, 11 (2017) 262.
50. M.-S. Tsai, C.-J. Lu, P.-G. Su, *Mater. Chem. Phys.*, 215 (2018) 293.
51. Ç. C. Koçak, S. Koçak, *Electroanal.*, 31 (2019) 1.
52. R. Huang, S. Chen, J. Yu, X. Jiang, *Ecotox. Environ. Safe.*, 184 (2019) 109619.
53. P. A. Raymundo-Pereira, N. O. Gomes, S. A.S. Machado, O.N. Oliveira Jr, *J. Electroanal. Chem.*, 848 (2019) 113319.